

A new multistable jerk system with Hopf bifurcations, its electronic circuit simulation and an application to image encryption

Abstract: In this work, we announce a new 3-D jerk system and show that it is chaotic and dissipative with the calculation of the Lyapunov exponents of the system. By performing a detailed bifurcation analysis, we observe that the new jerk system exhibits Hopf bifurcations. It is also shown that the new jerk system exhibits multistability behaviour with two coexisting chaotic attractors. An electronic circuit simulation of the jerk system is built using Multisim. Finally, we design a new approach to image encryption as a cryptographic application of our chaotic jerk system. The simulation outcomes prove the efficiency of the proposed encryption scheme with high security.

Keywords: Bifurcations; chaos; circuit design; jerk systems; image encryption.

1 Introduction

Systems modelling, computer design and engineering applications are some key areas of research in the computer science literature (Fan et al., 2020; Saba, 2020; Elyoussef et al., 2020; Singh et al., 2020; Azar et al., 2020a; Samy et al., 2020; Abouda et al., 2020; Essouifi and Achahbar, 2020; Feng et al., 2020; Zhinan et al., 2020; Azar et al., 2020b,c).

Chaos theory has several applications such as mechanical systems (Chang, 2020; Justin et al., 2020; Bi et al., 2020; Kaviya et al., 2020b), memristors (Yildirim, 2020; Escudero et al., 2020; Lai et al., 2020; Jahanshahi et al., 2020), neural networks (Du and Lu, 2021; Matsuki and Shibata, 2020; Akhmet et al., 2020; Liu et al., 2020), communication systems (Samimi et al., 2020; Al Bayati et al., 2020; Wu et al., 2020; Wang et al., 2020), lasers (Ashok et al., 2020; Bao et al., 2020; Zong et al., 2020; Kaviya et al., 2020a), etc.

In the recent years, good attention has been shown in the chaos literature on the modelling of jerk chaotic systems (Vaidyanathan et al., 2021; Sambas et al., 2021; Hua et al., 2020; Wen et al., 2020; Echenausía-Monroy et al., 2020). Vaidyanathan et al. (2021) proposed a dissipative jerk chaotic system with an egg-shaped strange attractor, and developed an electronic circuit using SPICE. Sambas et al. (2021) suggested a new jerk system with a saddle-focus balance point and designed an electronic circuit using Multisim. Hua et al. (2020) described two types of asymmetric memristor-based jerk circuits and constructed Multisim simulation models for the jerk circuits. Wen et al. (2020) studied a memristor-based jerk system with parametric excitation exhibiting complex bursting oscillations. Echenausía-Monroy et al. (2020) discussed fractional-order derivatives in a jerk system and implemented the associated electronic circuit using Multisim simulation model.

In mechanical systems, if $\nu(t)$ denotes the displacement of a particle or body, then $\dot{\nu}(t)$ represents its velocity, $\ddot{\nu}(t)$ its acceleration and $\dddot{\nu}(t)$ its jerk.

Jerk systems have many applications in science and engineering (Vaidyanathan, 2015; Joshi and Ranjan, 2020; Messias and Silva, 2020).

The general form of a third order autonomous jerk differential equation is given as

$$\dddot{\nu} = H(\nu, \dot{\nu}, \ddot{\nu}) \quad (1)$$

We note that the third order jerk ODE (1) can be expressed in an equivalent form as follows:

$$\begin{cases} \dot{x} = y, \\ \dot{y} = z, \\ \dot{z} = H(x, y, z) \end{cases} \quad (2)$$

This work elucidates a new 3-D jerk system having five nonlinear terms. Using Lyapunov exponent analysis, we establish that the new jerk system has chaoticity and dissipativity. We establish that the new jerk system undergoes Hopf bifurcations. We observe multistability in the new jerk system as it exhibits coexisting chaotic attractors.

Multi-stability is a special property of a chaotic system which means the existence of coexisting attractors for the same set of parameter values but different initial states. We show that the new chaotic jerk system exhibits multi-stability with coexisting chaotic attractors (Zhang et al., 2020; Zhou et al., 2020).

Using Multisim Version 13, we design an electronic circuit simulation of the proposed jerk system. Power spectral density analysis of the jerk circuit signals is also carried out using Multisim, which confirms chaos in the jerk circuit. Circuit design of a chaotic system is useful for real-world applications (Yildirim and Kacar, 2020; Wang et al., 2021; Rao et al., 2021).

Image encryption is an important area of research in communication theory that seeks to protect images from any unauthorised user access Abd-El-Atty et al. (2019). Image encryption is a widely used image protection technology and refers to reconstructing an image from

a recognizable manner into an unrecognizable manner Abd El-Latif et al. (2020); Abd EL-Latif et al. (2020).

Chaotic systems perform an important task in the design of encryption techniques because they are utilised to produce encryption key sequences Tsafack et al. (2020); Sambas et al. (2020). Chaotic maps are dynamical systems, whose behaviour is not only very sensitive to initial conditions but is also difficult to predict Abd-El-Atty et al. (2019).

In this work, based on the benefits of our presented chaotic jerk system, we propose a new approach to image encryption as a cryptographic application of our chaotic jerk system. Outcomes of experiments validate the efficiency of our presented encryption approach, while promising high efficiency for various cryptographic applications based on our jerk system.

2 A new jerk system

This section announces a new jerk system on the (x, y, z) -space with the dynamics

$$\begin{cases} \dot{x} = y \\ \dot{y} = z \\ \dot{z} = -z - ax^2z + bx^2 - c|x| - dy + xy^2 - x^3 \end{cases} \quad (3)$$

In the jerk dynamics (3), $X = (x, y, z)$ is the state and a, b, c, d are four positive constants.

It shall be shown in this section that the jerk system (3) depicts a self-excited, dissipative, chaotic attractor when the constants assume the values

$$a = 0.3, \quad b = 0.2, \quad c = 0.4, \quad d = 0.1 \quad (4)$$

The Lyapunov exponents of the jerk system (3) for the initial state $X(0) = (0.3, 0.1, 0.3)$ and parameter values as in (4) are numerically estimated using Wolf's algorithm (Wolf et al., 1985) for $1E5$ seconds in MATLAB as given below:

$$\tau_1 = 0.2542, \quad \tau_2 = 0, \quad \tau_3 = -2.4442 \quad (5)$$

The Kaplan-Yorke dimension of the chaotic jerk system (3) can be determined as follows:

$$D_{KY} = 2 + \frac{\tau_1 + \tau_2}{|\tau_3|} = 2.1040 \quad (6)$$

From the LE spectrum (5), it is deduced that $\tau_1 > 0$ and $\tau_1 + \tau_2 + \tau_3 = -2.19 < 0$.

Thus, the jerk system (3) has a dissipative, chaotic attractor in the (x, y, z) -space.

Figure 1 shows the MATLAB plots of the jerk system (3).

Multi-stability is a special property of a chaotic system which means the existence of coexisting attractors for the same set of parameter values but different initial states.

Figure 2 shows the multistability of the new chaotic system (1) with two coexisting attractors for $(a, b, c, d) = (0.3, 0.2, 0.4, 0.1)$ and the initial states $X_0 = (0.3, 0.1, 0.3)$ (blue trajectory) and $Y_0 = (-0.6, 0, -0.6)$ (red trajectory).

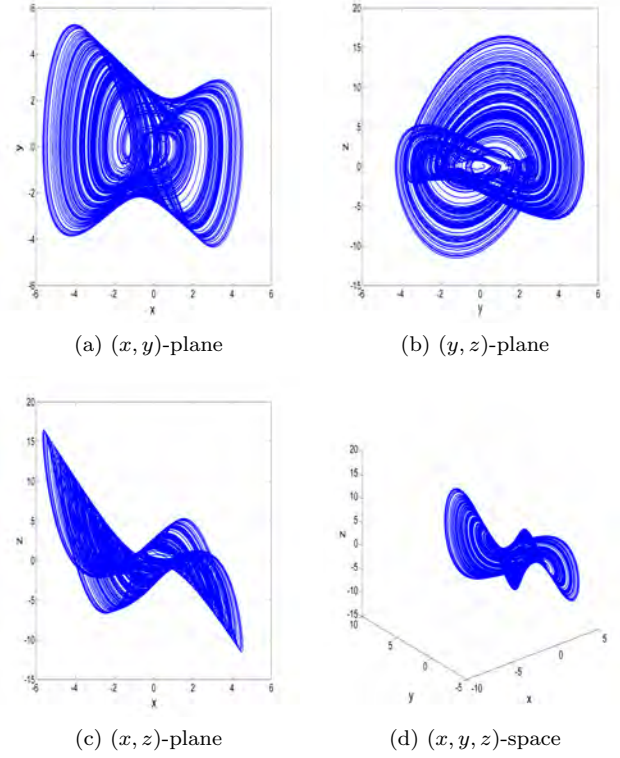


Figure 1: MATLAB plots of the new jerk system (3) for $X(0) = (0.3, 0.1, 0.3)$ and $(a, b, c, d) = (0.3, 0.2, 0.4, 0.1)$

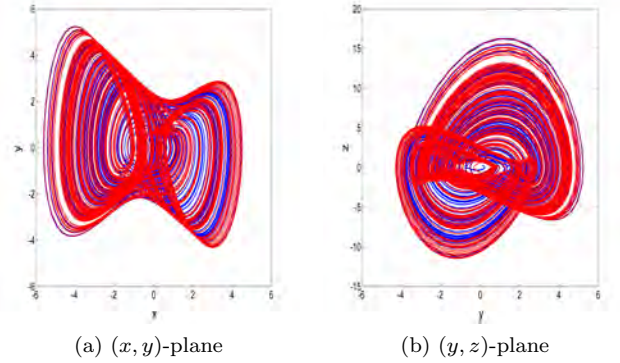


Figure 2: MATLAB plots showing multistability of the jerk system (3) with two coexisting chaotic attractors for $(a, b, c, d) = (0.3, 0.2, 0.4, 0.1)$ and the initial states $X_0 = (0.3, 0.1, 0.3)$ (blue trajectory) and $Y_0 = (-0.6, 0, -0.6)$ (red trajectory)

3 Bifurcation analysis of the jerk system

In this section, we perform a bifurcation analysis of the jerk system proposed in this work given by

$$\begin{cases} \dot{x} = y \\ \dot{y} = z \\ \dot{z} = -z - ax^2z + bx^2 - c|x| - dy + xy^2 - x^3 \end{cases} \quad (7)$$

The equilibrium states are found by setting the RHS of (7) to zero.

Thus, we solve the following system of equations:

$$y = 0 \quad (8a)$$

$$z = 0 \quad (8b)$$

$$-z - ax^2z + bx^2 - c|x| - dy + xy^2 - x^3 = 0 \quad (8c)$$

From (8a), $y = 0$.

From (8b), $z = 0$.

Putting $y = z = 0$ in (8a), we get the equation

$$bx^2 - c|x| - x^3 = 0 \quad (9)$$

We define the function $s(x) = \text{sign}(x)$. Thus, $s = 1$ when $x \geq 0$ and $s = -1$ when $x < 0$.

We can express the algebraic equation (9) as

$$x^3 - bx^2 + cs(x)x = x(x^2 - bx + cs) = 0 \quad (10)$$

Solving (10), we obtain three roots given by

$$x = 0, \quad x^2 - bx + cs = 0 \quad (11)$$

When $x = 0$, we obtain the trivial equilibrium $E_0 = (0, 0, 0)$ for the jerk system (7).

When $x \neq 0$, we solve the quadratic equation $x^2 - bx + cs = 0$.

Thus, there are two non-trivial equilibrium states for the jerk system (7) given by

$$x_e = \frac{1}{2}(b \pm \sqrt{b^2 - 4cs}) \quad (12)$$

Real-valued equilibrium states are therefore only possible when $b^2 - 4cs \geq 0$. Moreover, when $b^2 - 4c = 0$, the two equilibria, given by Eq. (12) coincide in a saddle-node bifurcation, and become $x_e = \frac{b}{2}$ (twice).

For examining the linear stability of the rest points, we first calculate the linearisation matrix of the jerk system (7):

$$J = \begin{pmatrix} 0 & 1 & 0 \\ 0 & 0 & 1 \\ 2bx - cs - 3x^2d - 1 - ax^2 \end{pmatrix}. \quad (13)$$

The characteristic equation of the matrix J is then obtained as

$$|J - \lambda I_3| = 0 \quad (14)$$

There are two cases:

- (i) When $x = 0$, we obtain the cubic characteristic equation:

$$\lambda^3 + \lambda^2 + \lambda d + cs = 0. \quad (15)$$

- (ii) If $x = x_e$, we obtain the characteristic equation:

$$\lambda^3 + (1 + ax_e^2)\lambda^2 + \lambda d + \Psi = 0, \quad (16)$$

where

$$\Psi = cs + 3x_e^2 - 2bx_e \quad (17)$$

3.1 Bifurcations

3.1.1 Trivial equilibrium state

When $c = 0$, Eq. (15) shows that a steady bifurcation, where $\lambda = 0$ is possible. The remaining eigenvalues are

$$\lambda = \frac{1}{2}(-1 \pm \sqrt{1 - 4d}). \quad (18)$$

When $d > 0$, both eigenvalues are either real and negative, or complex with a negative real part; this bifurcation is supercritical.

For a Hopf bifurcation, substituting $\lambda = i\omega$ into Eq. (15), equating real parts gives $\omega^2 = cs > 0$, and equating imaginary parts gives $\omega^2 = d > 0$.

For consistency we therefore require $cs = d$.

For $s = 1$ and $d = 0.1$, the Hopf bifurcation occurs when $c = 0.1$, with frequency $\omega = 0.3162$.

Using the standard results for the sum of the roots of a cubic equation, we see that the remaining eigenvalue must be $\lambda = -1$, and the Hopf bifurcation is supercritical.

Figure 3 shows the linear stability spectrum for the trivial equilibrium state for $0 \leq c \leq 1$. The Hopf bifurcation at $c = 0.1$ is clearly visible.

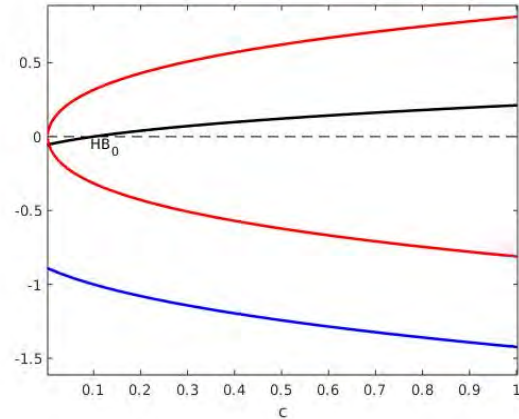


Figure 3: The linear eigenspectrum for the trivial equilibrium state for $0 \leq c \leq 1$. The blue curve shows the real eigenvalue, while the black and red curves show the real and imaginary parts of the complex conjugate eigenvalues. The Hopf bifurcation HB_0 at $c = 0.1$ is shown as the black curve crossing the dashed line through 0.

3.1.2 Non-trivial equilibrium states

When $c = 0$, Eq. (12) gives $x_e = 0, b$.

For $x_e = 0$, Eq. (16) gives the eigenvalues for the trivial equilibrium state. For $x_e = b$, Eq. (16) becomes

$$\lambda^3 + (1 + ab^2)\lambda^2 + \lambda d + b^2 = 0. \quad (19)$$

For the given set of parameter values, the roots are $\lambda = -0.9511$ and $\lambda = -0.0305 \pm 0.2028i$.

Figure 4 shows the eigenspectrum for $-1 \leq c \leq 1$.

There are two Hopf bifurcation points. One is at $c \approx -0.57$ with $\omega = 0.31633$, and the other is at $c \approx 0.033$ with $\omega = 0.31964$.

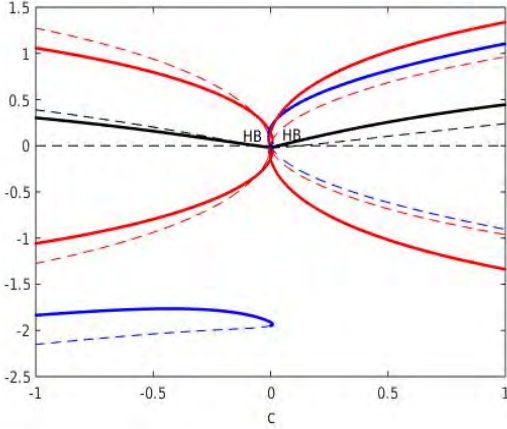


Figure 4: A bifurcation diagram of the real and complex eigenspectrum of Eq. (16) as c varies in $[-1, 1]$. There are 2 Hopf bifurcation points at which the real parts of the complex conjugate eigenvalues cross the imaginary axis at $c \approx 0.033$ and $c \approx -0.57$. The solid curves correspond to $x_e > 0$ and the dashed curves to $x_e < 0$. The colours are as in Figure 3.

3.2 Numerical Integrations

Figure 5 depicts a bifurcation transition plot of x_{max} as c varies, using the initial state $X_0 = (0.3, 0.1, 0.3)$. To produce this plot, we increased and decreased c from $c = -0.17$. There are two distinct regimes. When c is decreased, a chaotic region exists for $c < 0$, which undergoes period doubling bifurcations to a chaotic state. We were able to track this state as far as $c = -0.274$ before solutions became unbounded. The second regime again comprises period-doubling cascades, windows of periodicity, especially, the period-3 window, centred on $c = 0.5$, and chaotic states. Increasing c beyond $c = 0.748$ again resulted in unbounded states.

Figure 6 depicts the bifurcation transition plot of the x_{max} over each cycle as c increases and decreases from $c = 0.4$ for initial conditions $Y_0 = (-0.60, 0 - 0.6)$. Now there is only one branch of periodic and chaotic dynamics, which exists between $c = -0.144$ and $c = 0.748$. Again solution trajectories become unbounded outside this range of c .

4 Circuit model of the new jerk system

In this section, the new jerk system (3) is implemented with an electronic circuit. The simulation laboratory platform based on Multisim, Version 13. Circuit designs of chaotic jerk systems have many applications in engineering (Vaidyanathan et al., 2021; Sambas et al.,

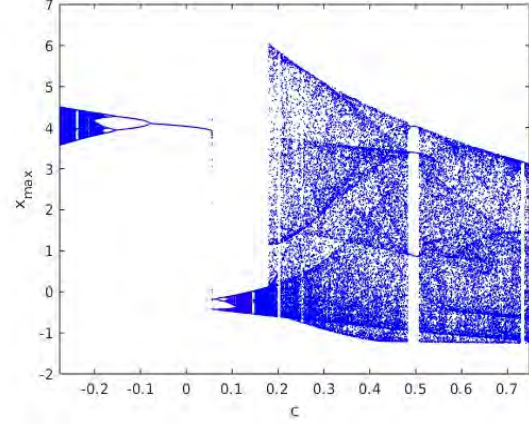


Figure 5: The bifurcation transition plot of x_{max} as c varies between $c = -0.274$ and $c = 0.748$, starting from $c = -0.17$ with initial conditions $X_0 = (0.3, 0.1, 0.3)$. Clearly shown are two separate chaotic and periodic regions.

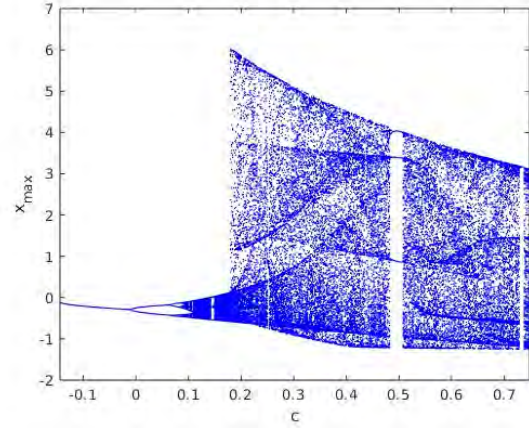


Figure 6: The bifurcation transition plot of x_{max} as c varies between $c = -0.144$ and $c = 0.748$, starting from $c = 0.4$ with initial conditions $X_0 = (-0.6, 0.0, -0.6)$. There is now only one region of chaotic and periodic behaviour.

2021; Hua et al., 2020; Wen et al., 2020; Echenausía-Monroy et al., 2020).

Figure 7 presents an analog circuit describing the new chaotic jerk system (3). The designed circuit includes 6 analog multipliers, 8 operational amplifiers, 20 resistors and 3 capacitors.

By using Kirchhoffs circuit laws, the circuitual equations of the designed circuit in Figure 7 are derived as follows:

$$\begin{aligned} C_1 \dot{x} &= \frac{1}{R_1} y \\ C_2 \dot{y} &= \frac{1}{R_2} z \\ C_3 \dot{z} &= -\frac{1}{R_3} z - \frac{1}{100R_4} x^2 z + \frac{1}{10R_5} x^2 - \frac{1}{R_6} |x| \\ &\quad - \frac{1}{R_7} y + \frac{1}{100R_8} xy^2 - \frac{1}{100R_9} x^3 \end{aligned} \quad (20)$$

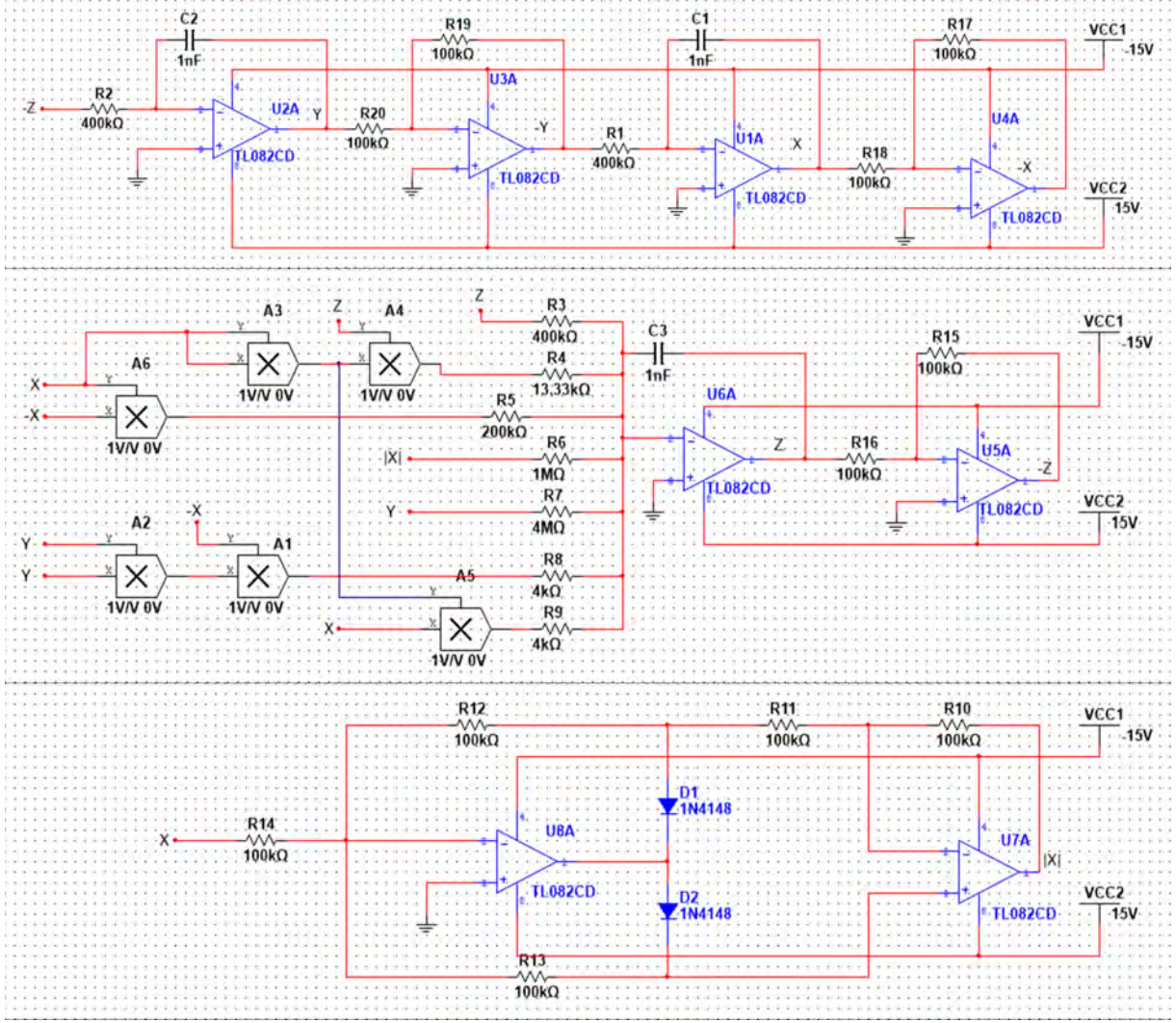


Figure 7: Circuit Design of the new chaotic jerk circuit (20)

The value of the resistors used in the circuit is as follows: $R_1 = R_2 = R_3 = 400 \text{ k}\Omega$, $R_4 = 13.33 \text{ k}\Omega$, $R_5 = 200 \text{ k}\Omega$, $R_6 = 1 \text{ M}\Omega$, $R_7 = 4 \text{ M}\Omega$, $R_8 = R_9 = 4 \text{ k}\Omega$, $R_{10} = R_{11} = R_{12} = R_{13} = R_{14} = R_{15} = R_{16} = R_{17} = R_{18} = R_{19} = R_{20} = 100 \text{ k}\Omega$, and $C_1 = C_2 = C_3 = 1 \text{ nF}$. The power supplies of all active devices are $\pm 15 \text{ Volts}$.

Figure 8 provides MultiSIM simulation results of the jerk circuit (20). The Multisim simulation results are consistent with the MATLAB simulation results of the jerk system (3) given in Figure 1.

Figure 9 shows the Fourier spectral analysis results for the three chaotic state signals X , Y and Z of the jerk circuit (20). The frequency range is 5 kHz, maximum peak 0.5 kHz. It corresponds to a prevailing frequency of the implementing oscillating loop. The power spectra of the produced signals are broadband, typical of chaotic signals.

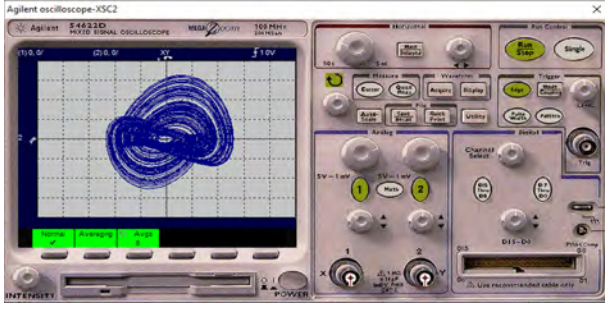
5 Image encryption algorithm using a modified jerk system

Chaotic systems play an important task in developing modern cryptographic purposes. Image encryption is an important area of research in communication theory that seeks to protect images from any unauthorised user access Abd-El-Atty et al. (2019). Image encryption is a widely used image protection technology and refers to reconstructing an image from a recognizable manner into an unrecognizable manner Abd El-Latif et al. (2020); Abd EL-Latif et al. (2020).

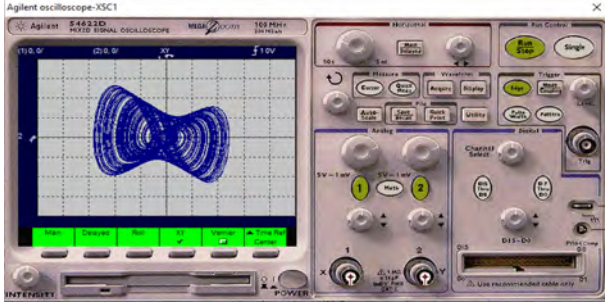
First, it is noted that we can derive a new chaotic jerk system by modifying the system dynamics in (3) as follows:

$$\begin{cases} \dot{x} = y \\ \dot{y} = z \\ \dot{z} = -z - ax^2z + bx^2 - c|y| - dy + xy^2 - x^3 \end{cases} \quad (21)$$

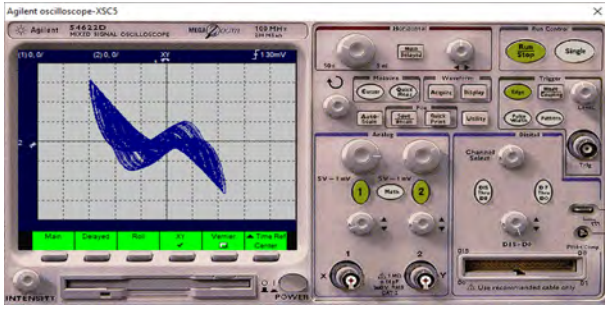
With the parameter set as $(a, b, c, d) = (0.3, 0.2, 0.3, 0.1)$ and initial state as $X(0) =$



(a) ((X, Y)-plane



(b) (Y, Z)-plane



(c) (X, Z)-plane

Figure 8: 2-D oscilloscope outputs of the new chaotic jerk circuit (20)

(0.3, 0.1, 0.3), the Lyapunov exponents (LE) values of the jerk system (21) are numerically evaluated for $1E5$ seconds in MATLAB as follows:

$$\psi_1 = 0.2385, \quad \psi_2 = 0, \quad \psi_3 = -2.3709 \quad (22)$$

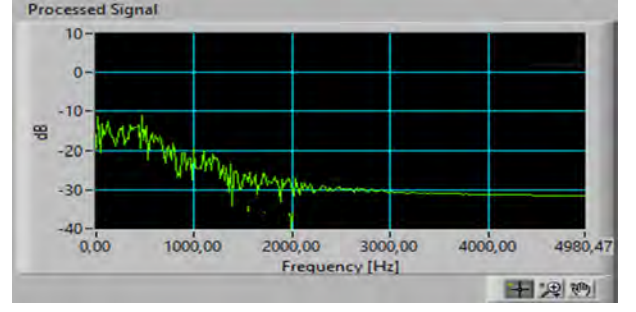
This confirms that the modified jerk system (21) is dissipative and chaotic.

In this section, we introduce our encryption approach based on the modified chaotic jerk system (21) and also provide the simulation results for the proposed encryption approach.

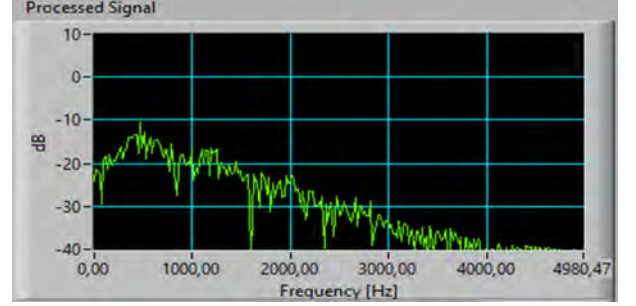
5.1 Proposed encryption approach

We propose a new approach to image encryption as a cryptographic application of our modified chaotic jerk system (21) in the discrete-time form as follows:

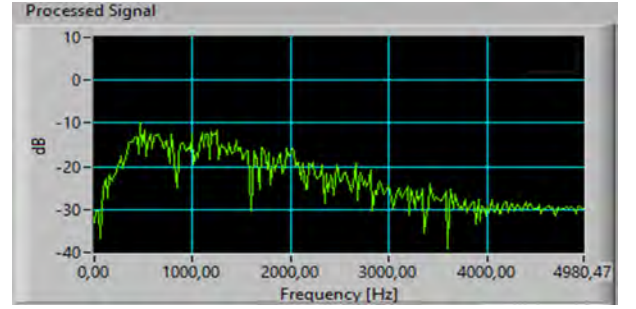
$$\begin{cases} x_{i+1} = (y_i) \bmod 1 \\ y_{i+1} = (z_i) \bmod 1 \\ z_{i+1} = (-z_i - ax_i^2 z_i + bx_i^2 - c|y_i| - dy_i + xy_i^2 - x_i^3) \bmod 1 \end{cases} \quad (23)$$



(a) X-signal



(b) Y-signal



(c) Z-signal

Figure 9: The spectral distribution of the new chaotic jerk circuit (20)

Concerning a plain image of dimensions $m \times n$, our modified chaotic jerk system is acted for $m \times n$ iterations for generating three sequences. The first two sequences are added to each other for generating one sequence used for permutating the plain image. Then the second sequence is added to the third sequence to produce a sequence used to substitute the permuted image. This step is repeated once by updating the initial conditions of our jerk system using information about the substituted image. The encryption procedure is outlined in Figure 10, while the specific steps of encryption are given as follows.

Step 1: Select values for initial conditions (x_0, y_0, z_0) and control parameters (a, b, c, d) for acting our chaotic jerk system $m \times n$ times to generate a three sequences $\{X_i\}$, $\{Y_i\}$, and $\{Z_i\}$, where $m \times n$ are the dimensions of the plain image I .

Step 2: Add the elements of sequence $\{X_i\}$ to the elements of sequence $\{Y_i\}$ for generating sequence $\{P_i\}$.

$$P_i = X_i + Y_i, \quad i = 1, 2, \dots, m \times n \quad (24)$$

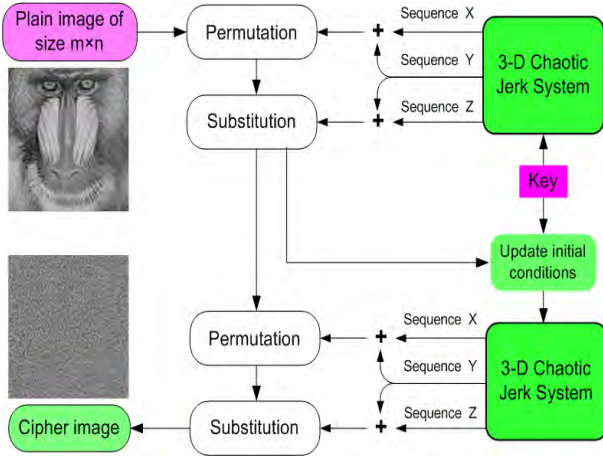


Figure 10: Block diagram of our encryption scheme.

Step 3: Sort the elements of sequence $\{P_i\}$ in ascending order to get the vector $\{Q_i\}$, and then obtain the index of every element of $\{P_i\}$ in $\{Q_i\}$ as a vector $\{QI_i\}$.

Step 4: Reshape the plain image I to a vector IV and then permute the vector image IV using the constructed vector QI .

$$PI(i) = IV(QI(i)), \quad i = 1, 2, \dots, m \times n \quad (25)$$

Step 5: Add the elements of sequence $\{Y_i\}$ to the elements of sequence $\{Z_i\}$ for generating sequence $\{S_i\}$, and then convert the sequence $\{S_i\}$ into integer values in the interval $[0, 255]$.

$$S_i = Y_i + Z_i, \quad i = 1, 2, \dots, m \times n \quad (26)$$

$$K_i = \text{fix}(S_i \times 10^{16}) \mod 256 \quad (27)$$

Step 6: Carry out bit-wise XOR process between the permuted vector PI and the generated key K to obtain the substituted vector SI .

$$SI_i = PI_i \oplus K_i, \quad i = 1, 2, \dots, m \times n \quad (28)$$

Step 7: Update the initial conditions (x_0, y_0, z_0) using some information about the substituted vector SI

$$\beta = \text{mod}(\text{sum}(SI), 256) / 256 \times 0.5 \quad (29)$$

$$x_0 = 0.5 \times x_0 + \beta \quad (30)$$

$$y_0 = 0.5 \times y_0 + \beta \quad (31)$$

$$z_0 = 0.5 \times z_0 + \beta \quad (32)$$

Step 8: Repeat the Steps from 1 to 6 using the updated initial values and substituted vector SI as vector IV . Then construct the final cipher image via reshaping the outcome of repeated steps SI as a matrix with dimensions $m \times n$.

5.2 Security and performance analysis

To validate the presented encryption approach, we utilized a laptop with Intel *Core™* i5-2450M CPU 2.5 GHz and RAM of 6 GB provided with MATLAB R2016b. Aeroplane, Sailboat, Boats, and Baboon are four images of size 512×512 which are used as test images (see Figure 11). Control parameters and primary conditions utilized for acting on our chaotic jerk system (21) are set as $x_0 = 0.3$, $y_0 = 0.1$, $z_0 = 0.3$, $a=0.3$, $b=0.2$, $c = 0.4$, and $d = 1.0$.

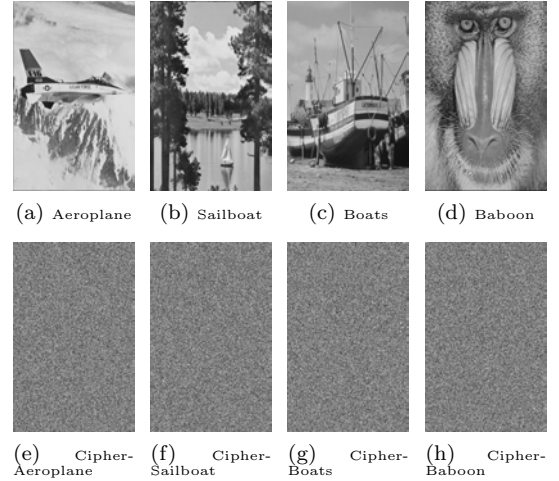


Figure 11: Dataset of images with dimension 512×512 and their corresponding ciphered images utilizing our proposed encryption mechanism.

5.2.1 Correlation analysis

One of the crucial tools used to estimate the significance of an image is to measure the correlation coefficient, which serves to provide a statistical measurement of the relationship between the original image and its encrypted one. The values of correlation coefficients for plain images are nearby 1 in each direction while in ciphered images by a reliable encryption method are nearby 0 (no relationship within neighbouring pixels) (Abd el Latif et al., 2020).

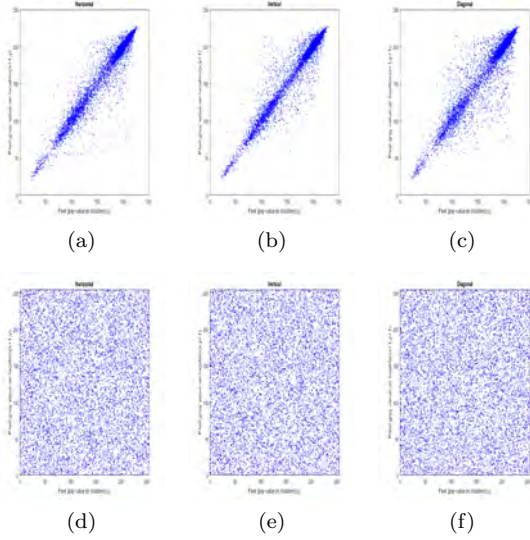
To measure the values of correlation coefficients for our presented approach, we picked randomly 10^4 pairs of neighbouring pixels per direction. Table 1 provides the outcomes of correlation coefficients in which the correlation values for ciphered images are very nearly zero. The correlation distribution of two neighbouring pixels in each direction for Aeroplane image is depicted in Fig. 12. From the outcomes provided in Table 1 and Fig. 12, no valuable information can be collected regarding the plain image by analysing the correlations of neighbourhood pixels.

5.2.2 Pixel change rate

To evaluate the outcome of two ciphered images for one plain image with tiny changes in pixel values, two

Table 1 Values of correlation coefficients for the experimented dataset

Image	Direction		
	Hor.	Ver.	Diag.
Aeroplane	0.9667	0.9695	0.9432
Cipher(Aeroplane)	0.0011	0.0004	0.0003
Sailboat	0.9727	0.9772	0.9603
Cipher (Sailboat)	-0.0008	0.0009	-0.0001
Boats	0.9796	0.9635	0.9480
Cipher (Boats)	-0.0012	-0.0006	0.0006
Baboon	0.7619	0.8654	0.7286
Cipher (Baboon)	-0.0001	-0.00001	0.0007

**Figure 12:** The correlation distribution of neighbouring pixels for Aeroplane image.

tests are utilized. The first measure is "Number of Pixels Changes Rate" (NPCR) and the other is "Unified Average Changing Intensity" (UACI), which are both expressed as given in (33) and (34), respectively.

$$NPCR = \frac{\sum_{i,j} D(i,j)}{M} \times 100\%, \quad (33)$$

$$D(i,j) = \begin{cases} 0 & \text{if } C_1(i,j) = C_2(i,j) \\ 1 & \text{if } C_1(i,j) \neq C_2(i,j) \end{cases}$$

$$UACI = \frac{1}{M} \left(\sum_{i,j} \frac{|C_1(i,j) - C_2(i,j)|}{2^N - 1} \right) \times 100\% \quad (34)$$

Here, C_1, C_2 indicate to the ciphered images for one plain image with tiny changes in pixel values, N indicates to the number of bits utilised to indicate the pixel value, and M indicates to the whole number of pixels in the image.

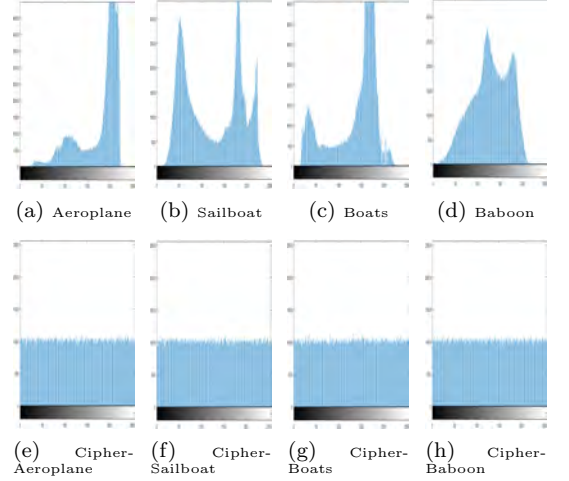
Table 2 provides the outcome of NPCR and UACI tools in which the average value for NPCR values is greater than 99.6%. Consequently, it follows that the proposed encryption approach is very sensitive to tiny pixel changes in the plain image.

Table 2 The outcomes of NPCR and UACI tests

Image	NPCR%	UACI%
Aeroplane	99.62044	33.46385
Sailboat	99.60479	33.36039
Boats	99.60518	33.57074
Baboon	99.61052	33.43163

5.2.3 Histogram test

Testing the histogram is an important measure for judging the effectiveness of an encryption method as it shows the frequency distribution of pixel values in an image. Any effective encryption approach must have identical histograms for distinct encrypted images to counteract various statistical attacks. Figure 13 shows the histograms of plain images that are distinct from each other, while the histograms of their analogue-encrypted images are identical. Consequently, our approach to encryption can withstand attacks on the histogram.

**Figure 13:** Histograms of plain and cipher images.

5.2.4 Information entropy

A different test to estimate the efficiency of our presented encryption approach is information entropy, which is a statistical test to evaluate the distribution of pixel values for per level in the image. The information entropy can be given as in (35).

$$E(X) = - \sum_{i=1}^{2^L-1} p(v_i) \log_2(p(v_i)) \quad (35)$$

Here $p(v_i)$ indicates to the probability of v_i . The possible values for a grey-scale image are 2^8 , so the ideal value of entropy is equal to 8-bit. Consequently, to assure the effectiveness of the proposed encryption approach, the values of entropy should be nearby to 8. The outcome of information entropy for plain images and their analogous ciphered ones are provided in Table 3,

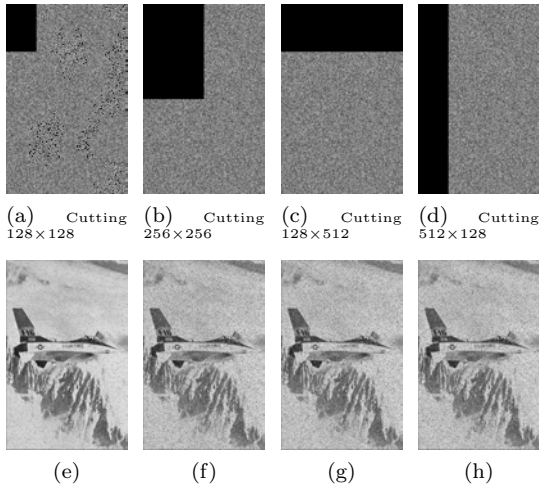
Table 3 The outcome of information entropy

Image	Plain image	Cipher image
Aeroplane	6.67765	7.99925
Sailboat	7.45696	7.99918
Boats	7.12375	7.99914
Baboon	7.35795	7.99932

which the entropy values for ciphered images are very nearby to 8.

5.2.5 Data loss attack

During the transmission of data over noisy carriers, it can be influenced by losing a part of the transmitted data Abd EL-Latif et al. (2020). So, a powerful encryption scheme must withstand data loss attacks. To assess our encryption method against data loss attacks, we cut out some information from the cipher image and then try to recover the data via the decryption method. Figure 14 shows the result of data loss attacks in which the original image restores successfully with no loss of information in the position of cutting part.

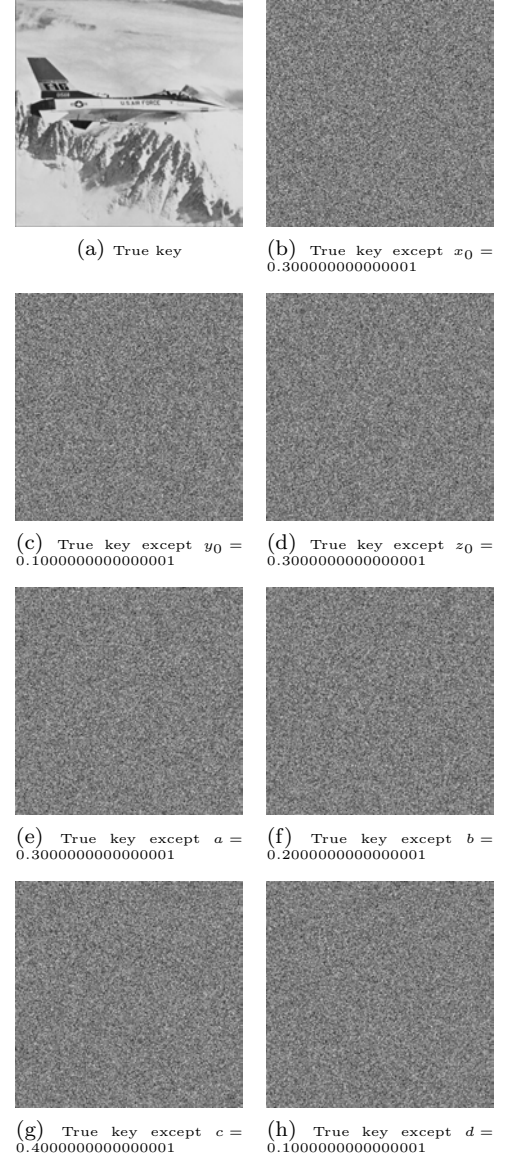
**Figure 14:** The consequence of data loss attack.

5.2.6 Key sensitivity

One of the crucial measures for any robust encryption techniques is key sensitivity. In order for the secure encryption algorithm to be reliable, any small variances in key parameters lead to huge variations in the deciphered image. To evaluate the key sensitivity of our presented method, we carried out the decryption process to the cipher image Aeroplane with various keys as explicated in Fig. 15.

6 Conclusions

In this work, we presented a new 3-D jerk system with a self-excited, dissipative, chaotic attractor. A

**Figure 15:** Key sensitivity for our cryptosystem, the cipher aeroplane image is deciphered with small variations in initial keys.

detailed bifurcation analysis showed that the new jerk system exhibits Hopf bifurcations. We also found that the new jerk system exhibits multistability behaviour with two coexisting chaotic attractors. An electronic circuit simulation of the jerk system was designed using Multisim for engineering applications. For the application of image encryption, we use a modified jerk system with dissipative chaotic attractor. Eventually, the benefits of our proposed 3D modified jerk chaotic system are utilised for designing a new image encryption approach. Simulation outcomes of our encryption approach with the modified jerk chaotic system proved the effectiveness of the proposed jerk system in various cryptographic applications.

References

- Abd-El-Atty, B., Abd El-Latif, A. A., and Venegas-Andraca, S. E. (2019). An encryption protocol for neqr images based on one-particle quantum walks on a circle. *Quantum Information Processing*, 18(9):272.
- Abd EL-Latif, A. A., Abd-El-Atty, B., Abou-Nassar, E. M., and Venegas-Andraca, S. E. (2020). Controlled alternate quantum walks based privacy preserving healthcare images in internet of things. *Optics & Laser Technology*, 124:105942.
- Abd el Latif, A. A., Abd-el Atty, B., Amin, M., and Ilyasu, A. M. (2020). Quantum-inspired cascaded discrete-time quantum walks with induced chaotic dynamics and cryptographic applications. *Scientific Reports*, 10(1):1–16.
- Abd EL-Latif, A. A., Abd-El-Atty, B., and Venegas-Andraca, S. E. (2020). Controlled alternate quantum walk-based pseudo-random number generator and its application to quantum color image encryption. *Physica A: Statistical Mechanics and its Applications*, 547:123869.
- Abd El-Latif, A. A., Abd-El-Atty, B., Venegas-Andraca, S. E., Elwahsh, H., Piran, M. J., Bashir, A. K., Song, O.-Y., and Mazurczyk, W. (2020). Providing end-to-end security using quantum walks in iot networks. *IEEE Access*, pages 92687–92696.
- Abouda, S. E., Abid, D. B. H., Elloumi, M., Koubaa, Y., and Chaari, A. (2020). Identification of non-linear stochastic systems using a new Hammerstein-Wiener neural network: a simulation study through a non-linear hydraulic process. *International Journal of Computer Applications in Technology*, 63(3):241–256.
- Akhmet, M., Seilova, R., Tleubergenova, M., and Zhamanshin, A. (2020). Shunting inhibitory cellular neural networks with strongly unpredictable oscillations. *Communications in Nonlinear Science and Numerical Simulation*, 89:105287.
- Al Bayati, B. M., Ahmad, A. K., and Al Naimee, K. A. (2020). Effect of control parameters on chaos synchronization by means of optical feedback. *Optics Communications*, 472:126032.
- Ashok, P., Ganesh Madhan, M., Deepiha, P., Rimmya, C., and Piramasubramanian, S. (2020). An efficient chaotic optical signal generation scheme using gain lever effect in bi-section laser diodes. *Optics Communications*, 475:126202.
- Azar, A. T., Anter, A. M., and Fouad, K. M. (2020a). Intelligent system for feature selection based on rough set and chaotic binary grey wolf optimisation. *International Journal of Computer Applications in Technology*, 63(1–2):4–24.
- Azar, A. T., Serrano, F. E., Rossell, J. M., Vaidyanathan, S., and Zhu, Q. (2020b). Adaptive self-recurrent wavelet neural network and sliding mode controller/observer for a slider crank mechanism. *International Journal of Computer Applications in Technology*, 63(4):273–285.
- Azar, A. T., Serrano, F. E., Rossell, J. M., Vaidyanathan, S., and Zhu, Q. (2020c). The construction and implementation of the positive-negative pressure pulse control system for oil well plug removal. *International Journal of Computer Applications in Technology*, 63(4):300–308.
- Bao, X., Li, Q., Wu, T., Deng, Y., Hu, M., and Zeng, R. (2020). WDM-based bidirectional chaotic communication for semiconductor lasers system with time delay concealment. *Optics Communications*, 472:125868.
- Bi, H., Qi, G., Hu, J., Faradja, P., and Chen, G. (2020). Hidden and transient chaotic attractors in the attitude system of quadrotor unmanned aerial vehicle. *Mathematics and Computers in Simulation*, 138:109815.
- Chang, S.-C. (2020). Stability analysis, routes to chaos, and quenching chaos in electromechanical valve actuators. *Mathematics and Computers in Simulation*, 177:140–151.
- Du, F. and Lu, J.-G. (2021). New criterion for finite-time synchronization of fractional order memristor-based neural networks with time delay. *Applied Mathematics and Computation*, 389:125616.
- Echenaúsía-Monroy, J., Gilardi-Velázquez, H., Jaimes-Reátegui, R., Aboites, V., and Huerta-Cuellar, G. (2020). A physical interpretation of fractional-order-derivatives in a jerk system: Electronic approach. *Communications in Nonlinear Science and Numerical Simulation*, 90:105413.
- Elyoussef, E. S., Martins, N. A., Bertol, D. W., Pieri, E. R. D., and Moreno, U. F. (2020). Simulation results and practical implementation of a PD-super-twisting second order sliding mode tracking control for a differential wheeled mobile robot. *International Journal of Computer Applications in Technology*, 63(3):213–227.
- Escudero, M., Vourkas, I., and Rubio, A. (2020). Alternative memristor-based interconnect topologies for fast adaptive synchronization of chaotic circuits. *Chaos, Solitons & Fractals*, 138:109974.
- Essouifi, M. and Achahbar, A. (2020). Discrete stochastic modelling of computer viruses prevalence on a reduced scale-free network. *International Journal of Computer Applications in Technology*, 63(3):257–271.

- Fan, R.-L., Chen, J.-A., Fei, Z.-N., Zhang, C.-Y., Yao, F.-H., and Wu, Q.-F. (2020). Neural network control and performance simulation of an active control mount with an oscillating coil actuator. *International Journal of Computer Applications in Technology*, 63(3):173–184.
- Feng, Z., Ying, G., and Hui, M. (2020). Experimental and modelling study on the response of mooring container ships in port under medium to long period waves. *International Journal of Computer Applications in Technology*, 62(4):327–337.
- Hua, M., Yang, S., Xu, Q., Chen, M., Wu, H., and Bao, B. (2020). Forward and reverse asymmetric memristor-based jerk circuits. *AEU - International Journal of Electronics and Communications*, 123:153294.
- Jahanshahi, H., Yousefpour, A., Munoz-Pacheco, J. M., Kacar, S., Pham, V., and Alsaadi, F. E. (2020). A new fractional-order hyperchaotic memristor oscillator: Dynamic analysis, robust adaptive synchronization, and its application to voice encryption. *Applied Mathematics and Computation*, 383:125310.
- Joshi, M. and Ranjan, A. (2020). An autonomous simple chaotic jerk system with stable and unstable equilibria using reverse sine hyperbolic functions. *International Journal of Bifurcation and Chaos*, 30(5). Article ID 2050070.
- Justin, M., Zdravković, S., Hubert, M. B., Betchewe, G., Doka, S. Y., and Kofane, T. C. (2020). Chaotic vibration of microtubules and biological information processing. *Biosystems*, 198:104230.
- Kaviya, B., Suresh, R., Chandrasekar, V., and Balachandran, B. (2020a). Influence of dissipation on extreme oscillations of a forced anharmonic oscillator. *International Journal of Non-Linear Mechanics*, 127:103596.
- Kaviya, B., Suresh, R., Chandrasekar, V. K., and Balachandran, B. (2020b). Influence of dissipation on extreme oscillations of a forced anharmonic oscillator. *International Journal of Non-Linear Mechanics*, 127:103596.
- Lai, Q., Wan, Z., Kuate, P. D. K., and Fotsin, H. (2020). Coexisting attractors, circuit implementation and synchronization control of a new chaotic system evolved from the simplest memristor chaotic circuit. *Communications in Nonlinear Science and Numerical Simulation*, 89:105341.
- Liu, Y., Xu, Y., and Ma, J. (2020). Synchronization and spatial patterns in a light-dependent neural network. *Communications in Nonlinear Science and Numerical Simulation*, 89:105297.
- Matsuki, T. and Shibata, K. (2020). Adaptive balancing of exploration and exploitation around the edge of chaos in internal-chaos-based learning. *Neural Networks*, 132:19–29.
- Messias, M. and Silva, R. (2020). Determination of nonchaotic behavior for some classes of polynomial jerk equations. *International Journal of Bifurcation and Chaos*, 30(8). Article ID 2050117.
- Rao, X.-B., Zhao, X.-P., Gao, J.-S., and Zhang, J.-G. (2021). Self-organizations with fast-slow time scale in a memristor-based Shinriki's circuit. *Communications in Nonlinear Science and Numerical Simulation*, 94. Article ID 105569.
- Saba, T. (2020). Skew decision process based on machine learning content analysis and clustering. *International Journal of Computer Applications in Technology*, 63(3):191–199.
- Sambas, A., Vaidyanathan, S., Tlelo-Cuautle, E., Abdel-Atty, B., El-Latif, A. A. A., Guillén-Fernández, O., Sukono, Hidayat, Y., and Gundara, G. (2020). A 3-D multi-stable system with a peanut-shaped equilibrium curve: Circuit design, FPGA realization, and an application to image encryption. *IEEE Access*, 8:137116–137132.
- Sambas, A., Vaidyanathan, S., Zhang, S., Mohamed, M. A., Zeng, Y., and Azar, A. T. (2021). A new 3-D chaotic jerk system with a saddle-focus rest point at the origin, its active backstepping control, and circuit realization. In Vaidyanathan, S. and Azar, A. T., editors, *Backstepping Control of Nonlinear Dynamical Systems*, Advances in Nonlinear Dynamics and Chaos (ANDC), pages 95 – 114. Academic Press.
- Samimi, M., Majidi, M. H., and Khorashadizadeh, S. (2020). Secure communication based on chaos synchronization using brain emotional learning. *AEU - International Journal of Electronics and Communications*, 127:153424.
- Samy, A., Hosny, K. M., and Zaied, A.-N. H. (2020). An efficient binary whale optimisation algorithm with optimum path forest for feature selection. *International Journal of Computer Applications in Technology*, 63(1–2):41–54.
- Singh, M. K., Saini, I., and Sood, N. (2020). A multi-functional BCI system for exigency assistance and environment control based on ML and IoT. *International Journal of Computer Applications in Technology*, 63(1–2):64–82.
- Tsafack, N., Sankar, S., Abdel-Atty, B., Kengne, J., Jithin, K. C., Belazi, A., Mehmood, I., Bashir, A. K., Song, O., and EL-Latif, A. A. A. (2020). A new chaotic map with dynamic analysis and encryption application in internet of health things. *IEEE Access*.

- Vaidyanathan, S. (2015). Analysis, control, and synchronization of a 3-D novel jerk chaotic system with two quadratic nonlinearities. *Kyungpook Mathematical Journal*, 55(3):563–586.
- Vaidyanathan, S., Pham, V.-T., and Azar, A. T. (2021). A new chaotic jerk system with egg-shaped strange attractor, its dynamical analysis, backstepping control, and circuit simulation. In Vaidyanathan, S. and Azar, A. T., editors, *Backstepping Control of Nonlinear Dynamical Systems*, Advances in Nonlinear Dynamics and Chaos (ANDC), pages 53 – 71. Academic Press.
- Wang, B., Zhang, B., and Liu, X. (2021). An image encryption approach on the basis of a time delay chaotic system. *Optik*, 225. Article ID 165737.
- Wang, M., Wang, X., Wang, C., Xia, Z., Zhao, H., Gao, S., Zhou, S., and Yao, N. (2020). Spatiotemporal chaos in cross coupled map lattice with dynamic coupling coefficient and its application in bit-level color image encryption. *Chaos, Solitons & Fractals*, 139:110028.
- Wen, Z., Li, Z., and Li, X. (2020). Bursting dynamics in parametrically driven memristive jerk system. *Chinese Journal of Physics*, 66:327 – 334.
- Wolf, A., Swift, J., Swinney, H., and Vastano, J. (1985). Determining Lyapunov exponents from a time series. *Physica D: Nonlinear Phenomena*, 16(3):285–317.
- Wu, T., Li, Q., Bao, X., and Hu, M. (2020). Time-delay signature concealment in chaotic secure communication system combining optical intensity with phase feedback. *Optics Communications*, 475:126042.
- Yildirim, M. (2020). DNA encoding for RGB image encryption with memristor based neuron model and chaos phenomenon. *Microelectronics Journal*, 104:104878.
- Yildirim, M. and Kacar, F. (2020). Chaotic circuit with OTA based memristor on image cryptology. *AEU - International Journal of Electronics and Communications*, 127. Article ID 153490.
- Zhang, X., Li, C., Chen, Y., IU, H., and Lei, T. (2020). A memristive chaotic oscillator with controllable amplitude and frequency. *Chaos, Solitons and Fractals*, 139. Article ID 110000.
- Zhinan, W., Gangjun, Z., and Yong, C. (2020). Prediction on hydroelastic responses of very large floating structure with the eigenfunction expansion-matching method. *International Journal of Computer Applications in Technology*, 62(4):338–347.
- Zhou, W., Wang, G., Iu, H., Shen, Y., and Liang, Y. (2020). Complex dynamics of a non-volatile memcapacitor-aided hyperchaotic oscillator. *Nonlinear Dynamics*, 100(4):3937–3957.
- Zong, J., Hajomer, A. A., Zhang, L., Hu, W., and Yang, X. (2020). Real-time secure optical OFDM transmission with chaotic data encryption. *Optics Communications*, 473:126005.